

---

# Towards an Understanding of Neural Networks in Natural-Image Spaces

---

Yifei Fan and Anthony Yezzi

School of Electrical and Computer Engineering  
Georgia Institute of Technology

yifei@gatech.edu, ayezzi@ece.gatech.edu

## Abstract

Two major uncertainties, dataset bias and perturbation, prevail in state-of-the-art AI algorithms with deep neural networks. In this paper, we present an intuitive explanation for these issues as well as an interpretation of the performance of deep networks in a natural-image space. The explanation consists of two parts: the philosophy of neural networks and a hypothetic model of natural-image spaces. Following the explanation, we slightly improve the accuracy of a CIFAR-10 classifier by introducing an additional “random-noise” category during training. We hope this paper will stimulate discussion in the community regarding the topological and geometric properties of natural-image spaces to which deep networks are applied.

## 1 Introduction

Recent years have witnessed the rapid development of artificial intelligence (AI) and deep learning. Deep networks distinguish themselves in various types of computer-vision challenges such as ImageNet (Deng et al., 2009) and COCO (Lin et al., 2014), and some AI algorithms even outperform humans on certain tasks and test sets (Stallkamp et al., 2012), (Schroff et al., 2015). However, two major issues remain and prevent us from establishing robust real-world applications with current algorithms. One is dataset bias (Torralba and Efros, 2011), meaning that a machine-learning algorithm that performs well on one dataset may fail on another. The other is perturbation (Szegedy et al., 2013), which shows that tiny modifications on inputs may lead to incorrect outputs by deep networks, even though the perturbations are almost imperceptible to humans.

In this paper, we present our understanding of neural networks in natural-image spaces and manage to explain the uncertainties. Contributions of this paper follow:

- We provide intuitive explanations on dataset bias and perturbations, the two prevailing uncertainties in neural networks.
- We demonstrate that the values of training samples differ. Random noise, surprisingly, contains a certain amount of information and improves the performance of neural-network classifiers.

The rest of the paper is organized as follows. Section 2 reviews related studies. Section 3 illustrates the philosophy of neural networks, demonstrates that the training process is data-dependent and zero-constrained, and specifies the flaw from limited options in data usage. Section 4 examines the characteristics of image data and presents the hypothetic image-space model. Sections 5 and 6 follow with experiments and discussion, respectively. All relevant materials that accompany this paper are available on GitHub<sup>1</sup>.

## 2 Related Work

**Dataset bias:** The dataset bias issue was first pointed out in Torralba and Efros (2011), after the authors became aware that researchers who had worked in object and scene recognition could easily guess which images came from which dataset. They claimed that such a difference among datasets could even be captured by a classifier and reflected in the diagonal pattern of the confusion matrix. Although the purpose of computer vision datasets is to offer unbiased representations of the world, they seem to express them with a strong build-in bias. A follow-up study (Khosla et al., 2012) exploited dataset

<sup>1</sup><https://github.gatech.edu/yfan88/neural-network-in-image-space>

bias during the training phase. The authors proposed two sets of weights, bias vectors and visual world weights to undo the damage of dataset bias. In conclusion, the authors pointed the benefit of explicitly accounting for bias when multiple datasets are involved. Another study (Tommasi et al., 2014) provided a large-scale analysis of the issue with twelve databases. However, as most previous studies have addressed the issue on dataset level, they do not help explain or eliminate such a bias in practice. It is possible that the data samples we collect resemble multiple datasets to some extent. Thus, stating the characteristics of images that lead to such bias is beneficial. One apparent bias stems from the size of targets. The evaluation metric of COCO (Lin et al., 2014) challenges, which emphasizes the effects of iconic and non-iconic objects, accounts for the size factor.

**Perturbation:** As an intriguing property first discovered by Szegedy et al. (2013), a hardly-perceptible perturbation on inputs could lead to misclassification. Since then, researchers have been working on methods of attacking/fooling or defending deep networks. On the attackers' side, the authors of Nguyen et al. (2015) forced the network to generate high-confidence predictions for images that are even unrecognizable by humans. With DeepFool (Moosavi-Dezfooli et al., 2016b), we can easily change the output label for an image with unnoticeable perturbations. Furthermore, we can fool the network with very few pixels (Su et al., 2017). In general, two types of perturbations exist: adversarial and universal (Moosavi-Dezfooli et al., 2017). While the former depends on individual image, the latter is a uniform perturbation applied to all images. The existence of universal perturbation implies important characteristics of the geometry of the decision boundaries in high-dimensional space (Moosavi-Dezfooli et al., 2016a). In Mopuri et al. (2017), universal perturbations are computed without any knowledge of the target data. On the defenders' side, efficient defenses against adversarial attacks are provided in Zantedeschi et al. (2017). The idea is to stabilize the prediction by reinforcing the weak points of the network. A recent study (Madry et al., 2017) proposed methods for training networks with improved resistance to adversarial attacks. In practice, studies do not agree on the extent of the effects of these attacks. Perturbations for object detection in autonomous vehicles is not a concern (Lu et al., 2017). New attacks, however, generate more subtle adversarial examples (Evtimov et al., 2017). Nevertheless, combat between attackers and defenders will guide us to more robust and secure networks.

**Image manifold:** The idea of the image manifold comes from smooth manifold in mathematics (Lee, 2003). A topological space  $M$  is a topological  $n$ -manifold if it is 1) a Hausdorff space, 2) second countable, and 3) locally

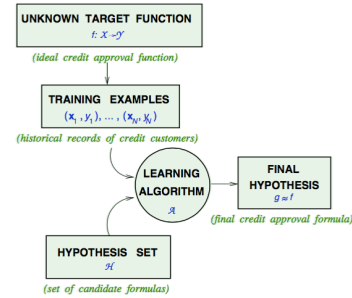


Figure 1: Machine learning scheme, from on-line lecture notes by Professor Yaser Abu-Mostafa

Euclidean of dimension  $n$ . Manifold  $M$  has important topological properties, including the following: 1) It is connected if and only if it is path connected, and 2) it is locally compact. It is assumed that natural images are embedded in a manifold whose dimension is much lower than that of the images themselves. Such a formulation consists of two key components: a distance metric and a map from parameter (or feature, latent) space to the image space. In computer vision, researchers manage to approximate the image manifold via learning (He et al., 2004). The generative adversarial network (GAN) is used in the state-of-the-art approximation of the image manifold (Zhu et al., 2016). However, such approximation may not fully account for that spaces of images are vast and sparsely populated (Hassabis et al., 2017).

### 3 Philosophy of Neural Networks

#### 3.1 Ambiguity of Tasks

We start with a high-level scheme for machine learning, as shown in Figure 1. Starting from an empirical hypothesis, machine-learning algorithms manage to “learn” an underlying unknown target function with the help of training data. One constraint for such a paradigm is that the objective must be a *function*. In mathematics, a function is “a relation between a set of inputs and a set of outputs with the property that each input is related to *exactly one output*.” Figure 2 shows the classification of functions. Relations with multiple outputs for an input, although extremely common in our daily life, are not functions. While humans are extremely good at handling such relations (e.g., Facebook friends and LinkedIn connections), computers cannot directly express relations with arithmetic/logic operations.

One major advantage of deep convolutional neural networks is that their structure helps convert a relation to functions. Compared with classic machine-learning algorithms, convolution generates much more features for

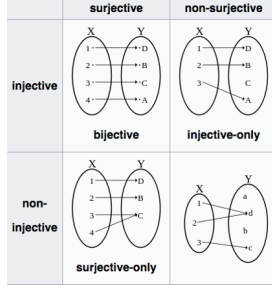


Figure 2: Types of functions (from Wikipedia): injective, surjective and bijective,

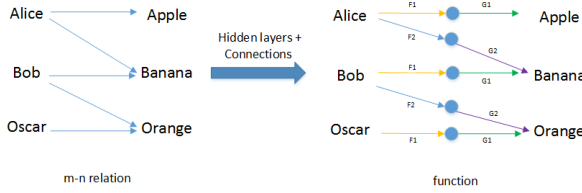


Figure 3: Conversion of an  $m$ - $n$  relation to functions.  $G_1 \circ F_1(p)$ : find the fruit that starts with the same letter as your name. The right-hand side has learnable injections.

inputs, and hidden layers ensure injection. Figure 3 illustrates such conversion. However, the degree of similarity to a mathematical function varies among tasks. Based on past experience and our understanding, we make the following conjecture.

**Conjecture.** *Suppose there exists a metric that measures similarity, especially with respect to the uniqueness of the output for each given input, between a task and a mathematical function. We claim that for tasks that highly resemble mathematical functions, machine-learning algorithms tend to be more accurate.*

For instance, since detection can be decomposed as localization and classification (Sermanet et al., 2013), it possesses higher ambiguity than its sub-tasks. The conjecture also agrees with the argument that vision problems such as output predictions may be less ambiguous than graphics tasks (Isola et al., 2016).

### 3.2 Learning in the View of Calculus of Variation

In this section, we analyze the computation of neural networks and reveal that the training process is **data-dependent**. Most computation is based on the gradient descent (Cauchy, 1847): If  $f(\cdot)$  is defined and differentiable in the neighborhood of point  $a$ , then  $f(x)$  decreases fastest if one goes from  $a$  in the direction of the negative gradient of  $f$  at  $a$  (i.e.,  $-\nabla f(a)$ ). In other words, if  $a^{n+1} = a^n - \gamma \nabla f(a^n)$  for small enough  $\gamma$ , then  $f(a^n) \geq f(a^{n+1})$ . As a result, neural networks

are likely to find the extremum point of  $f(\cdot)$ . However, one crucial difference exists between the function  $f(\cdot)$  and that in Figure 1. Here  $f(\cdot)$  is the objective function that we maximize/minimize. After iterations, we obtain an extremum point  $a^*$  and its corresponding extremum  $f(a^*)$ . In contrast, according to functional analysis, the  $f(\cdot)$  in Figure 1 is an extremum point similar to  $a^*$ , which can be interpreted as an infinite-dimensional vector indexed<sup>2</sup> by its domain  $X$ , that is,  $(f_x)_{x \in X}$ . Obtaining the final hypothesis of the underlying target function  $f(\cdot)$  requires a loss function/functional  $L(f(\cdot))$ .

In calculus of variation, a functional is a special type of function that takes another function as its input. An example of a functional is as follows.

$$L(f, x) = \int_0^1 f(x) dx \quad (1)$$

In a discrete manner, a functional appears to be the following.

$$MSE = \frac{1}{m} \sum_{i=1}^m (f(x_i) - y_i)^2 \quad (2)$$

The output of a functional depends on both the *integrand/summand*  $f(\cdot)$  and the *integral* for integration/summation. Therefore, the training process is heavily data-dependent, and deficiencies in data themselves and data usage will impact learning-based algorithms. Furthermore, based on the *Universal Approximation Theorem* (Csaji, 2001), the “infinite-dimensional vector”  $f(\cdot)$  can be approximated with deep networks in a finite number of terms. Similar to Taylor series expansion, more terms tend to achieve more accurate approximation, which implies that deeper networks will be favored. Empirical results from Urban et al. (2016) agree with the implication.

### 3.3 The Achilles’ Heel of Machine Learning

Most canonical tutorials on neural networks discretize the “infinite-dimensional vector”  $f(\cdot)$  immediately after introducing the idea of *gradient descent*. The advantage is that everything becomes computable. However, we lose sight of the machine-learning scheme, which consists of two steps: 1) designing a loss function that fully represents the objective of the task, such as the cycle loss reported in Zhu et al. (2017); and 2) solving for the extremum of the loss function to obtain the desired target function, such as the method found in Haeffele and Vidal (2017).

We introduce the *point-function duality* of target functions to emphasize that the training process is **zero-constrained**. From the point perspective,  $f(\cdot)$ , as a point

<sup>2</sup>E.g., the index set of  $v = (v_1, v_2, v_3)$  is  $\{1, 2, 3\}$

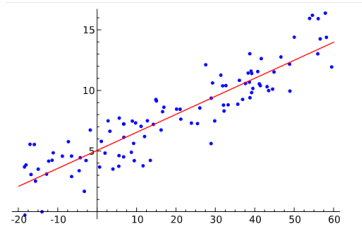


Figure 4: Linear regression: can  $x$  or  $y$  take arbitrary values?

in the domain of loss functional  $L(f)$ , cannot determine what its actual domain and range are. From the function perspective, the topological property of its domain and range matters, especially if we apply  $f : X \rightarrow Y$  to other inputs. For example, the linear regression in Figure 4 fits the curve by minimizing square errors. However, the obtained function, different from admissible functions, sets no restrictions on the value of  $x$  or  $y$ . In some cases, the target function might be locally linear around training data. As equation (2) suggests, the output of the loss function depends on input data  $\{x\}$  as well. If the function is trained using data within a certain neighborhood, dataset bias will occur. Figure 5 shows the curve fitting results of the following function with default settings but different training data.

$$f(x) = \begin{cases} 0, & x \leq 0.5 \\ 1, & x > 0.5 \end{cases}$$

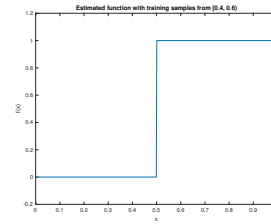
Similarly, the decision boundaries for images will shift as training samples differ. Therefore, instead of resulting from insufficient data, dataset bias is an **intrinsic** property of the machine learning scheme.

### 3.4 The Logic of Neural Networks

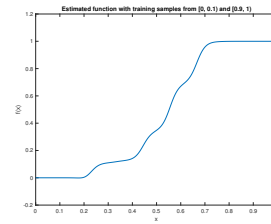
When you have eliminated all which is impossible, then whatever remains, however improbable, must be the truth.

Sherlock Holmes

We claim that perturbations are related to a flaw in current data usage, that is, *limited options*. Let's put ourselves in the shoes of neural networks and rethink the reason for perturbations. Although outputs change after perturbation, networks may not be fooled. The output vector from a neural-network classifier indicates the probabilities that the input belongs to the corresponding categories. Suppose we have 1,000 categories, and the input belongs to category 1. After perturbation, the predicted label shifts from category 1 to 2. Instead of asserting that the network is attacked, we need to admit that



(a) Fitting with 40,000 uniformly distributed samples from  $[0.4, 0.6]$



(b) Fitting with uniformly distribute samples from  $[0, 0.1)$  and  $(0.9, 1)$ , 20,000 for each

Figure 5: The impact of different training samples in curve fitting

the network still outputs correct probabilities for most but not all of the remaining categories. In this sense, the network is “innocent” as the “winner-takes-all” rule of picking the label with the maximum likelihood is specified by network designers.

We analyze perturbations from a completely opposite perspective. During training, neural networks not only learn what an object “is” but also capture what “is not” an instance of a category. The mechanism of successful perturbations is to meet the criteria of “is not.” When a classifier eliminates all impossible categories with Sherlock Holmes’ logic, it has to pick the remaining category as the final output. Usually and unfortunately, no category for exceptions exists. Consequently, the classifier assumes that the target function is defined on all samples from the input space, which is rarely true. In addition, to classify the input space smoothly, the decision boundaries are deformed. Figure 6 presents an interesting experiment in which the pretrained AlexNet (Krizhevsky et al., 2012) was asked to classify hybrid images<sup>3</sup> (Oliva et al., 2006) composed of high-frequency component of one image and low-frequency component of the other. Under current rules, the classifier has to choose one of the category from 1,000 available options.

**Remark.** *One possible reason for the existence of perturbation is that the classifier has limited options.*

<sup>3</sup>Selected from [https://www.cc.gatech.edu/classes/AY2016/cs4476\\_fall/results/proj1/](https://www.cc.gatech.edu/classes/AY2016/cs4476_fall/results/proj1/)

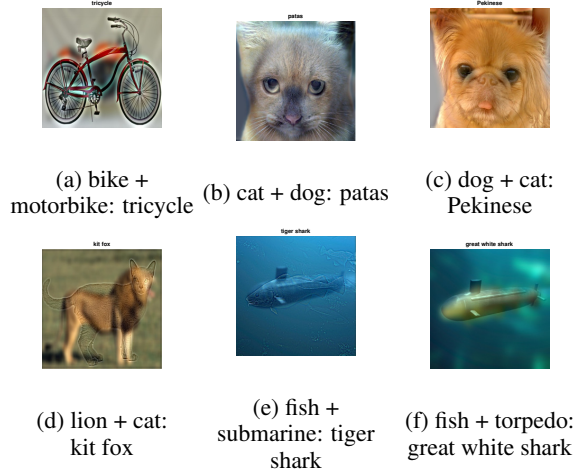


Figure 6: Classification for hybrid images

## 4 Model of Natural-image Spaces

Since training is data-dependent, we deem that the characteristics of the input space are worth studying. In this section, we study the topological and geometric property of the natural-image spaces, as well as their consequences on computer vision algorithms using neural networks. The most related studies are image generation and translation with generative adversarial networks (Goodfellow, 2016).

### 4.1 Image Manifold in a Discrete Form

Before the deep-learning era, most classical computer-vision algorithms started from the continuous world by building features with physical meaning. Researchers have studied mappings from the image space to a target space, to solve tasks such as classification and segmentation. Because of recent developments in computation, estimating the reverse mapping, or even to traverse the image manifold (Zhu et al., 2016) is possible. However, there is no guarantee that all important topological and geometric properties in continuous are preserved in such a discrete estimation unless we have a complete picture of the image space. In fact, although GANs can generate plenty of amazing images, the failure cases remain uncontrollable and sometimes difficult to explain. To match the discrete settings in GAN, we address natural image spaces in a completely discrete manner, hoping that we will gain a better understanding of current algorithms.

**Definition 4.1.** Natural-image space: Let  $\mathbb{Z}_{[l,u]}$  denote the set of integers from  $l$  to  $u$ . Given an image  $I$  with resolution  $w \times h$  and  $d$  channels, the image is considered as a point of the  $\mathbb{Z}_{[0,255]}^{w \times h \times d}$ -based natural image space  $\mathbb{I}^{w \times h \times d}$  if  $I$  appears to be natural according to the perfect dis-

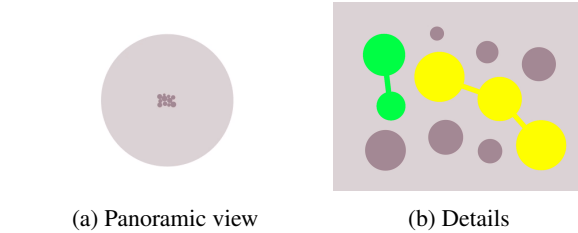


Figure 7: Illustration on the connectivity of natural image space. Points represent natural images.

criminator.

### 4.2 Properties of Natural-image Spaces

In this subsection, we will describe what natural-image spaces look like by listing its important properties.

#### 4.2.1 Sparsity

We first consider the probability that a random sample in  $\mathbb{Z}_{[0,255]}^{w \times h \times d}$  falls on the corresponding natural-image space  $\mathbb{I}^{w \times h \times d}$ . Even for gray-scale images with a resolution of  $16 \times 16$ , we have  $256^{256} = 2^{2048} \approx 10^{614}$  possible cases. The number of natural images, however, tends to be much smaller. Thus, natural images are similar to stars in the universe in which “the emptiness is normal, and the richness of images’ neighborhood is the exception.”<sup>4</sup>

#### 4.2.2 Connectivity

Based on the sparsity, we infer that two images in the natural image spaces are not always “path connected”<sup>5</sup> through adjacent grid points in  $\mathbb{Z}_{[0,255]}^{w \times h \times d}$ . In other words, we may not be able to traverse between two arbitrary images via a path of natural images. A natural-image space can be regarded as a *quotient space* consisting of numerous equivalence classes of path-connected images. Figure 7 shows the conceptual model of natural-image spaces in which each small darker circle represents a natural image, and connections between two circles imply that one can be derived from another (e.g., using filters).

#### 4.2.3 Scale-space effect

When image resolution rises, the total number of cases increases exponentially. Similar to the effect in scale-space theory (Lindeberg, 1994), humans are more sensitive to images with higher resolutions than to those with lower resolutions, meaning that flaws in high resolutions

<sup>4</sup>Adapted from *Powers of Ten* by IBM

<sup>5</sup>A discrete version of path connectedness in algebraic topology

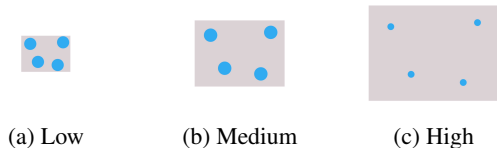


Figure 8: Illustration of the scale-space effect of natural-image spaces at various resolutions

tend to be identified more easily. Hence, we make the following conjecture: Natural-image spaces are denser in lower resolutions. Meanwhile, we assume that the quantity of valid natural images increases more slowly than that of possible cases, which indicates that it is more probable that a random image will fall in natural-image spaces in lower resolutions. The conjecture is consistent with results that show algorithms for image generation and translation appear to be more natural in images with relatively low resolutions. The scale-space property of natural-image spaces is illustrated in Figure 8.

### 4.3 Reinterpretation of Recent Work

We explain existing work from the viewpoint of this paper. While image translation can be interpreted as finding a mapping between two points in a natural-image space, image generation seeks the reverse mapping from a latent space to a natural-image space. The major difficulty lies in the need for **designing an appropriate loss functional that indirectly regulates the performance of its extremum** (i.e., the target function). Effective approaches are found in recent studies such as those in Isola et al. (2016) and Zhu et al. (2017). Specifically,  $L_1$  norm forces the image to be sufficiently sharp, which prevents the output from leaving a natural-image space. Strict rules for coloring adopted by the facade dataset (Tyleček and Šára, 2013) limits the cases of outputs, leading to a denser output space. Cycle loss manages to ensure the bidirectional property of the mapping, so that it obtains a more stable bijection. In Karras et al. (2017), the network first locates natural-image clusters in lower resolutions, which is easier as Figure 8 suggests. With these coarse locations, outputs in higher resolutions are more likely to stay on natural-image spaces. The network then grows the scale progressively to refine outputs for better details. In Zheng et al. (2016), stability-loss guarantees that the target function is locally consistent within the neighborhood of each image, providing buffer zones between images and decision boundaries. The authors of Metzén et al. (2017) proposed a subnetwork that distinguishes genuine data from perturbed ones, shrinking the natural-image spaces for the subsequent classifier. By assigning weights to training data, RetinaNet (Lin et al., 2017) detects objects more accurately at a fast speed.

Metric	Explanation
$A$	Average test accuracy
$\sigma_A$	Standard deviation of test accuracy
$P_c$	Average confidence of correctly classified samples
$P_s$	Average spuriousness of misclassified samples
$P_g$	Average probability of the ground-truth category for misclassified samples

Table 1: Evaluation metrics used in experiments

## 5 Experiments

Here we present experimental results that support our statements on the impact of training samples and the benefits of utilizing the topological and geometric properties of natural-image spaces. Since classification is the basis for advanced tasks, we set up CIFAR-10 (Krizhevsky and Hinton, 2009) image classification experiments with a neural network adapted from the example code provided by MATLAB<sup>6</sup>. To demonstrate the effect of training samples, we design the experiments in a controlled manner and follow default configurations on the neural networks. For each experiment, we obtain final results by averaging results of 50 executions with fixed training data. Table 1 describes the evaluation metric. We assume that the probability of each category is negatively correlated with the distance from the sample to the centroid of that category.

### 5.1 Impact of Training Samples

After training, we categorized the training samples into two classes: those that were correctly classified by the classifier and those that were misclassified by the classifier. We further sorted correctly-classified samples according to their confidence and select two subgroups with relatively higher ( $S_{hc}$ ) and lower confidences ( $S_{lc}$ ), respectively. Similarly, we further selected two subgroups with higher spuriousness ( $S_{hs}$ ) and lower spuriousness ( $S_{ls}$ ) from the misclassified training samples. With all subgroups the same size, we then retrained the network with the selected subgroups to illustrate the impact of different training samples. Table 2 shows the performance of the classifier after retraining with subgroups of the original training data.

We observe the following on Table 2. High-confidence images are required for higher test accuracy, especially when a limited number of training samples are provided. Highly spurious images are misleading when the size of the training set is small; as the training set expands, however, such adverse images become valuable and lead to even higher accuracy than training with

<sup>6</sup><https://www.mathworks.com/help/vision/examples/object-detection-using-deep-learning.html>

Training set	$A$	$\sigma_A$	$P_c$	$P_s$	$P_g$
$S_{lc}^{.25} \cup S_{ls}^{.25}$	27.12%	2.40%	26.56%	22.91%	14.65%
$S_{lc}^{.25} \cup S_{hs}^{.25}$	19.26%	0.92%	24.68%	22.86%	13.67%
$S_{hc}^{.25} \cup S_{ls}^{.25}$	53.61%	1.23%	79.67%	58.00%	12.73%
$S_{hc}^{.25} \cup S_{hs}^{.25}$	51.49%	1.29%	66.57%	44.77%	14.57%
$S_{lc}^{.50} \cup S_{ls}^{.50}$	52.16%	1.58%	45.73%	36.39%	18.61%
$S_{lc}^{.50} \cup S_{hs}^{.50}$	41.07%	1.18%	35.11%	30.86%	17.99%
$S_{hc}^{.50} \cup S_{ls}^{.50}$	65.78%	0.58%	88.08%	70.23%	11.41%
$S_{hc}^{.50} \cup S_{hs}^{.50}$	60.48%	0.67%	75.62%	50.50%	15.92%
$S_{lc}^{.75} \cup S_{ls}^{.75}$	68.76%	1.16%	74.25%	52.34%	18.36%
$S_{lc}^{.75} \cup S_{hs}^{.75}$	60.55%	1.31%	58.33%	43.00%	20.33%
$S_{hc}^{.75} \cup S_{ls}^{.75}$	70.81%	0.31%	92.67%	76.09%	10.28%
$S_{hc}^{.75} \cup S_{hs}^{.75}$	70.85%	0.47%	80.45%	55.76%	16.24%
$S_{lc}^{.80} \cup S_{ls}^{.80}$	70.89%	0.92%	77.04%	54.94%	17.79%
$S_{lc}^{.80} \cup S_{hs}^{.80}$	64.12%	1.08%	60.99%	46.06%	20.09%
$S_{hc}^{.80} \cup S_{ls}^{.80}$	71.43%	0.36%	92.65%	76.73%	10.16%
$S_{hc}^{.80} \cup S_{hs}^{.80}$	71.75%	0.54%	82.45%	56.57%	16.32%

Table 2: Performance of the classifier retrained with subgroups of training data.  $S_c^p$ : the top  $p$  of training samples selected with criteria  $c$

low-spuriousness ones. One possible explanation is that highly spurious images, as outliers, force the network to adjust, which lowers loss. In this sense, the highly spurious images contain higher entropy (more information) than low-spuriousness images after a certain number of iterations. Classifiers trained with  $S_{hc} \cup S_{ls}$  are determined (smaller  $\sigma_A$ ) and confident (higher  $P_c$ ,  $P_s$ ) about what they predict, regardless of whether they are right or wrong. By contrast, classifiers trained with  $S_{lc} \cup S_{hs}$  are relatively hesitant (larger  $\sigma_A$ ) in that the average probabilities for the output category ( $P_c$ ,  $P_s$ ) are lower; moreover, even if the prediction is wrong, they still assign a certain probability on the ground-truth category ( $P_g$ ). In summary, the results demonstrate that the performance of classifiers depends on the training data. In other words, dataset bias occurs even within the same dataset because it is an intrinsic property of the learning scheme.

## 5.2 Training with a Random-Noise Class

Adding random noise samples to training data is the easiest way to change the topology of the input space. The use of random noise in training neural networks dates back to the 1990s. Researchers have injected noise into inputs and weights to improve the generalization (Matsuoka, 1992), avoid local minima, and speed up back-propagation (Wang and Principe, 1999). A recent study (Zheng et al., 2016) used random perturbation to stabilize the networks. However, researchers have never treated random noise as independent training samples containing information that can be directly employed for training neural networks. In this work, we add an extra category of random noise as negative samples, retrain the

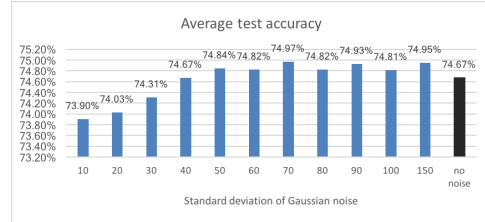


Figure 9: Average test accuracy of networks trained with additional random-noise samples with different standard deviations

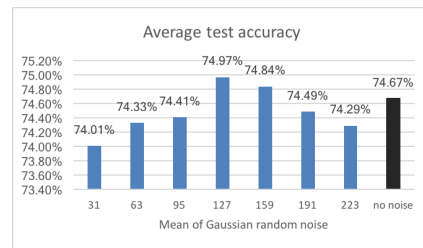


Figure 10: Average test accuracy of networks trained with additional random-noise samples with fixed standard deviation 70 and different means

network, and test the classifier on the original test set that does not contain samples of random noise. Surprisingly, with random noise, we slightly improve the test accuracy at almost no extra cost except slightly longer computation time.

We start testing with the most-common Gaussian random noise under four controlling parameters: mean, standard deviation, quantity, and scale (correlation among pixels). We design the experiments in a controlled manner to evaluate the effect of each factor. Figure 9 shows that Gaussian random noise improves test accuracy as long as the standard deviation is sufficiently large. As the standard deviation increases, Gaussian noise becomes more uniformly distributed. Figure 10 shows that Gaussian random noise centered at the middle of the intensity range outperforms others. Figure 11 shows that test accuracy varies with different numbers of random-noise training samples. This finding suggests that random noise might contain a certain amount of information that could teach the classifier what “is not” a natural image. Such information, however, becomes saturated as the number of random-noise samples increases. With an excessive number (e.g.,  $100\times$ ) of noise samples, neural networks may become overwhelmed, spending much longer time in training but obtaining little enhancement. Figure 12 demonstrates the effect of scale in Gaussian random noise. Experiments with uniformly distributed random noise return results in a similar pattern (please

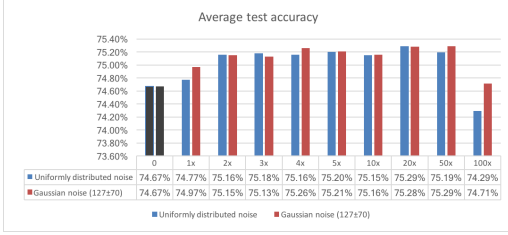


Figure 11: Average test accuracy with different numbers of random-noise training samples ( $1 \times := 5000$  samples)

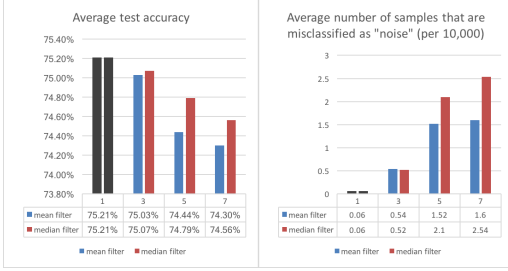


Figure 12: Performance of networks that are trained with additional Gaussian noise in different scales

refer to the supplementary materials). We simulate the variation of scales using median and mean filters with different sizes. As the scale of random noise increases, the performance of the classifier deteriorates.

We further repeat the experiments in Table 2 with the additional category of uniformly distributed random-noise training samples, and report results in Table 3. Similar results with Gaussian random noise are provided in the supplementary materials. Comparing Tables 2 and 3, we observe following. Training classifiers with random noise tends to increase test accuracy, but such an effect is more obvious with fewer training samples. Despite the introduction of a new risk of “misclassification as random noise”, it vanishes as the number of training images increases. Generally speaking, classifiers trained with random noise tend to be more determinant (higher  $P_c$ ,  $P_s$ , lower  $\sigma_A$ ); surprisingly, for misclassified samples, the probability of the ground-truth category also increases (higher  $P_g$ ).

The motivation of adding random noise is to change the topology of natural-image space by specifying the invalid zones that do not belong to the space. As a result, if we subtract the region of random noise from the input space of the classifier, then the input space is no longer “dense” and has more holes. Geometrically, to avoid such holes, random noise tends to push the decision boundaries towards the centroid of each category. Figure 13 provides a simplified illustration. In addition, feeding neural networks with random-noise samples that

Training set	$A$	$\sigma_A$	$P_c$	$P_s$	$P_g$	$N$
$S_{lc}^{.25} \cup S_{ls}^{.25}$	30.82%	2.11%	28.31%	24.14%	15.43%	2.1
$S_{lc}^{.25} \cup S_{hs}^{.25}$	21.32%	0.91%	25.27%	23.40%	14.30%	1.08
$S_{hc}^{.25} \cup S_{ls}^{.25}$	55.27%	0.86%	79.24%	58.60%	12.86%	5.36
$S_{hc}^{.25} \cup S_{hs}^{.25}$	53.26%	1.06%	67.22%	44.81%	14.87%	2.78
$S_{lc}^{.50} \cup S_{ls}^{.50}$	53.11%	1.36%	46.70%	37.26%	19.23%	0.9
$S_{lc}^{.50} \cup S_{hs}^{.50}$	40.82%	1.10%	35.05%	31.23%	18.55%	0.68
$S_{hc}^{.50} \cup S_{ls}^{.50}$	66.37%	0.53%	88.56%	70.03%	11.61%	1.12
$S_{hc}^{.50} \cup S_{hs}^{.50}$	65.13%	0.65%	76.10%	50.47%	16.16%	0.72
$S_{lc}^{.75} \cup S_{ls}^{.75}$	70.03%	0.81%	73.88%	53.26%	18.42%	0.14
$S_{lc}^{.75} \cup S_{hs}^{.75}$	61.95%	1.38%	54.95%	43.80%	20.69%	0.50
$S_{hc}^{.75} \cup S_{ls}^{.75}$	71.05%	0.54%	92.43%	75.64%	10.54%	0.22
$S_{hc}^{.75} \cup S_{hs}^{.75}$	71.42%	0.55%	80.94%	55.75%	16.48%	0.34

Table 3: Performance of the classifier retrained with subgroups of training data, with  $5 \times$  uniformly distributed random noise.  $S_c^p$ : the top  $p$  of training samples selected with criteria  $c$ .  $N$ : the average number of test samples that are misclassified as “noise” per 10,000

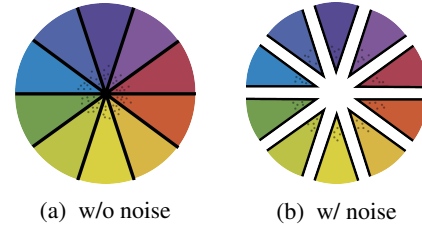


Figure 13: Conceptual model of an image space: Darker dots in the center are training samples. Black lines are decision boundaries. The white gap in (b) is noise.

are completely unnatural can help them learn what “is not” an object. However, as the scale of Gaussian noise increases, more pixels are correlated and samples become less unnatural. Therefore, the effect is weakened by Gaussian noise with larger correlations among pixels.

Finally, we report two cases that lead to interesting results. In one case, the test accuracy drops if we train the classifier with images of solid colors. The set of solid-color images can be interpreted as an embedded sub-hyperplane that 1) has the same or even lower dimension as decision boundaries, and 2) spreads across the entire input space. Classifying such sets in lower dimensions is difficult because their boundaries reside in even lower dimensions. For a better understanding, we may consider solving a curve-fitting problem with classification instead of regression. In the other case, test accuracy also drops in cases of Gaussian random noise with various means, standard deviations, and scales. Such mixed samples come from several separated clusters in the input space. Since neural networks group samples into path-connected regions (Fawzi et al., 2017), mixed noise tends to be a more difficult case.

## 6 Discussion

The primary contribution of this paper is the intrinsic explanation of uncertainties in neural networks that are applied to images. The explanation also guides the experiment design. In contrast, the results of the experiments are just the tip of the iceberg. As the training process is data-dependent and zero-constrained, the learned classifier may suffer from dataset bias. Several key topological and geometric properties of smooth manifolds are missing in the discrete natural-image spaces adopted by neural networks, which we believe is the reason for perturbation as well as baffling outcomes from image translation and generation. Under current settings, the networks take it for granted that natural-image spaces are dense and simply return the most-likely output from limited options. Restrictions on the input domain and output range of neural networks are lacking. Experiment results suggest that adding an additional category of negative training data to handle exceptions is helpful. These phenomena lead to the following questions: What compositions of data are better for training more robust classifiers and detectors? How do we measure the value or impact of training samples?

We hope the paper will stimulate discussion in the community regarding the intrinsic properties of the input space to which deep networks are applied. Open problems include the entropy of training samples, features of the decision boundaries, and the equivalence relation for images. Understanding the topological and geometric properties of natural-image spaces with a rigorous model will help us interpret the performance of state-of-the-art deep neural networks. Moreover, it may provide a more comprehensive understanding of the theoretical basis for deep neural networks. In practice, we may enhance the performance of neural networks by improving the quality of training samples or altering how we use data.

### Acknowledgements

Yifei Fan would like to thank Dr. James Hays for the inspiring discussion in CS 7476 and the chance to present part of the work in class.

### References

Cauchy, A. (1847). Méthode générale pour la résolution des systèmes d'équations simultanées. *Comp. Rend. Sci. Paris*, 25(1847):536–538.

Csáji, B. C. (2001). Approximation with artificial neural

networks. *Faculty of Sciences, Eötvös Loránd University, Hungary*, 24:48.

Deng, J., Dong, W., Socher, R., Li, L.-J., Li, K., and Fei-Fei, L. (2009). Imagenet: A large-scale hierarchical image database. In *Computer Vision and Pattern Recognition, 2009. CVPR 2009. IEEE Conference on*, pages 248–255. IEEE.

Evtimov, I., Eykholt, K., Fernandes, E., Kohno, T., Li, B., Prakash, A., Rahmati, A., and Song, D. (2017). Robust physical-world attacks on machine learning models. *arXiv preprint arXiv:1707.08945*.

Fawzi, A., Moosavi-Dezfooli, S.-M., Frossard, P., and Soatto, S. (2017). Classification regions of deep neural networks. *arXiv preprint arXiv:1705.09552*.

Goodfellow, I. (2016). Nips 2016 tutorial: Generative adversarial networks. *arXiv preprint arXiv:1701.00160*.

Haeffele, B. D. and Vidal, R. (2017). Global optimality in neural network training. In *The IEEE Conference on Computer Vision and Pattern Recognition (CVPR)*.

Hassabis, D., Kumaran, D., Summerfield, C., and Botvinick, M. (2017). Neuroscience-inspired artificial intelligence. *Neuron*, 95(2):245–258.

He, X., Ma, W.-Y., and Zhang, H.-J. (2004). Learning an image manifold for retrieval. In *Proceedings of the 12th annual ACM international conference on Multimedia*, pages 17–23. ACM.

Isola, P., Zhu, J.-Y., Zhou, T., and Efros, A. A. (2016). Image-to-image translation with conditional adversarial networks. *arXiv preprint arXiv:1611.07004*.

Karras, T., Aila, T., Laine, S., and Lehtinen, J. (2017). Progressive growing of gans for improved quality, stability, and variation. *arXiv preprint arXiv:1710.10196*.

Khosla, A., Zhou, T., Malisiewicz, T., Efros, A. A., and Torralba, A. (2012). Undoing the damage of dataset bias. In *European Conference on Computer Vision*, pages 158–171. Springer.

Krizhevsky, A. and Hinton, G. (2009). Learning multiple layers of features from tiny images.

Krizhevsky, A., Sutskever, I., and Hinton, G. E. (2012). Imagenet classification with deep convolutional neural networks. In *Advances in neural information processing systems*, pages 1097–1105.

Lee, J. M. (2003). Smooth manifolds. In *Introduction to Smooth Manifolds*, pages 1–29. Springer.

Lin, T.-Y., Goyal, P., Girshick, R., He, K., and Dollár, P. (2017). Focal loss for dense object detection. *arXiv preprint arXiv:1708.02002*.

- Lin, T.-Y., Maire, M., Belongie, S., Hays, J., Perona, P., Ramanan, D., Dollár, P., and Zitnick, C. L. (2014). Microsoft coco: Common objects in context. In *European conference on computer vision*, pages 740–755. Springer.
- Lindeberg, T. (1994). Scale-space theory: A basic tool for analyzing structures at different scales. *Journal of applied statistics*, 21(1-2):225–270.
- Lu, J., Sibai, H., Fabry, E., and Forsyth, D. (2017). No need to worry about adversarial examples in object detection in autonomous vehicles. *arXiv preprint arXiv:1707.03501*.
- Madry, A., Makelov, A., Schmidt, L., Tsipras, D., and Vladu, A. (2017). Towards deep learning models resistant to adversarial attacks. *arXiv preprint arXiv:1706.06083*.
- Matsuoka, K. (1992). Noise injection into inputs in back-propagation learning. *IEEE Transactions on Systems, Man, and Cybernetics*, 22(3):436–440.
- Metzen, J. H., Genewein, T., Fischer, V., and Bischoff, B. (2017). On detecting adversarial perturbations. *arXiv preprint arXiv:1702.04267*.
- Moosavi-Dezfooli, S.-M., Fawzi, A., Fawzi, O., and Frossard, P. (2016a). Universal adversarial perturbations. *arXiv preprint arXiv:1610.08401*.
- Moosavi-Dezfooli, S.-M., Fawzi, A., Fawzi, O., Frossard, P., and Soatto, S. (2017). Analysis of universal adversarial perturbations. *arXiv preprint arXiv:1705.09554*.
- Moosavi-Dezfooli, S.-M., Fawzi, A., and Frossard, P. (2016b). Deepfool: a simple and accurate method to fool deep neural networks. In *Proceedings of the IEEE Conference on Computer Vision and Pattern Recognition*, pages 2574–2582.
- Mopuri, K. R., Garg, U., and Babu, R. V. (2017). Fast feature fool: A data independent approach to universal adversarial perturbations. *arXiv preprint arXiv:1707.05572*.
- Nguyen, A., Yosinski, J., and Clune, J. (2015). Deep neural networks are easily fooled: High confidence predictions for unrecognizable images. In *Proceedings of the IEEE Conference on Computer Vision and Pattern Recognition*, pages 427–436.
- Oliva, A., Torralba, A., and Schyns, P. G. (2006). Hybrid images. In *ACM Transactions on Graphics (TOG)*, volume 25, pages 527–532. ACM.
- Schroff, F., Kalenichenko, D., and Philbin, J. (2015). Facenet: A unified embedding for face recognition and clustering. In *Proceedings of the IEEE Conference on Computer Vision and Pattern Recognition*, pages 815–823.
- Sermanet, P., Eigen, D., Zhang, X., Mathieu, M., Fergus, R., and LeCun, Y. (2013). Overfeat: Integrated recognition, localization and detection using convolutional networks. *arXiv preprint arXiv:1312.6229*.
- Stallkamp, J., Schlipsing, M., Salmen, J., and Igel, C. (2012). Man vs. computer: Benchmarking machine learning algorithms for traffic sign recognition. *Neural networks*, 32:323–332.
- Su, J., Vargas, D. V., and Kouichi, S. (2017). One pixel attack for fooling deep neural networks. *arXiv preprint arXiv:1710.08864*.
- Szegedy, C., Zaremba, W., Sutskever, I., Bruna, J., Erhan, D., Goodfellow, I., and Fergus, R. (2013). Intriguing properties of neural networks. *arXiv preprint arXiv:1312.6199*.
- Tommasi, T., Tuytelaars, T., and Caputo, B. (2014). A testbed for cross-dataset analysis. *arXiv preprint arXiv:1402.5923*.
- Torralba, A. and Efros, A. A. (2011). Unbiased look at dataset bias. In *Computer Vision and Pattern Recognition (CVPR), 2011 IEEE Conference on*, pages 1521–1528. IEEE.
- Tyleček, R. and Šára, R. (2013). Spatial pattern templates for recognition of objects with regular structure. In *German Conference on Pattern Recognition*, pages 364–374. Springer.
- Urban, G., Geras, K. J., Kahou, S. E., Aslan, O., Wang, S., Caruana, R., Mohamed, A., Philipose, M., and Richardson, M. (2016). Do deep convolutional nets really need to be deep and convolutional? *arXiv preprint arXiv:1603.05691*.
- Wang, C. and Principe, J. C. (1999). Training neural networks with additive noise in the desired signal. *IEEE Transactions on Neural Networks*, 10(6):1511–1517.
- Zantedeschi, V., Nicolae, M.-I., and Rawat, A. (2017). Efficient defenses against adversarial attacks. *arXiv preprint arXiv:1707.06728*.
- Zheng, S., Song, Y., Leung, T., and Goodfellow, I. (2016). Improving the robustness of deep neural networks via stability training. In *Proceedings of the IEEE Conference on Computer Vision and Pattern Recognition*, pages 4480–4488.
- Zhu, J.-Y., Krähenbühl, P., Shechtman, E., and Efros, A. A. (2016). Generative visual manipulation on the natural image manifold. In *European Conference on Computer Vision*, pages 597–613. Springer.
- Zhu, J.-Y., Park, T., Isola, P., and Efros, A. A. (2017). Unpaired image-to-image translation using cycle-consistent adversarial networks. *arXiv preprint arXiv:1703.10593*.